Dipole condensates in synthetic rank-2 electric fields

Jiali Zhang,[1] Wenhui Xu,[2] Qi Zhou,[2,3,*] and Shaoliang Zhang[1,4,†]

[1] *School of Physics, International Joint Laboratory on Quantum Sensing and Quantum Metrology, Center for Intelligence and Quantum Science, Huazhong University of Science and Technology, Wuhan 430074, China*
[2] *Department of Physics and Astronomy, Purdue University, West Lafayette, IN, 47907, USA*
[3] *Purdue Quantum Science and Engineering Institute, Purdue University, West Lafayette, IN 47907, USA*
[4] *Hubei Key Laboratory of Gravitation and Quantum Physics, Institute for Quantum Science and Engineering, Huazhong University of Science and Technology, Wuhan 430074, China*

(Dated: September 19, 2025)

Dipole condensates, formed from particle-hole pairs, represent a unique class of charge-neutral quantum fluids that evade conventional vector gauge fields, making their electrodynamic responses difficult to probe in natural materials. Here, we propose a tunable platform using strongly interacting two-component ultracold atoms to realize dipole condensates and probe their coupling to rank-2 electric fields. By applying spin-dependent forces and treating spin as a synthetic dimension, we engineer a synthetic rank-2 electric field that induces measurable electrodynamic responses. We identify the atomic analog of perfect Coulomb drag: increasing intercomponent interactions leads to equal and opposite displacements of the centers of mass of the two spin components. Furthermore, a rank-2 electric field imprints a phase twist in the dipole condensate and generates a supercurrent of dipoles that obeys the dipolar Josephson relation—a smoking gun for dipole condensation. Our results establish a powerful platform for exploring dipolar superfluidity under tensor gauge fields.

Whereas bosons tend to form a condensate at low temperatures, they may condense by unusual means. Composite particles formed by multiple bosons—including particle-hole pairs—can themselves undergo condensation [1–10]. A primary example is the exciton condensates observed in a variety of solid or organic materials [11–20]. Another example is found in the dipole Bose-Hubbard model, which supports a dipolar condensate as the ground state in certain parameter regimes [21–26]. Additionally, certain non-equilibrium dynamics have been shown to dynamically generate dipole condensates [26].

Due to their charge-neutrality, dipoles are insensitive to ordinary vector gauge fields. For instance, a uniform electric field cannot induce a net dipole current, rendering dipole condensates effectively insulating [27, 28]. To elicit electrodynamic responses, higher-rank tensor gauge fields are required [29–34]. In the study of exciton condensates in bi-layer systems, Coulomb drag has been employed [35–37]. Applying an electric field to one layer induces a counterflow in the other due to the presence of strong interlayer Coulomb interactions. This phenomenon can be interpreted as a manifestation of a rank-2 tensor electric field [26].

Despite significant progress in understanding exciton condensates and Coulomb drag, fundamental challenges remain unresolved. One of the most pressing issues is the lack of direct detection of phase coherence in solids. While transport measurements such as Coulomb drag suggest coherent behavior between electrons and holes, these signatures are often indirect and can be influenced by competing effects such as disorder. For instance, recent experiments reported the observation of perfect Coulomb drag but finite resistance remains [38, 39]. Direct evidence for phase coherence of exciton condensates remains elusive. It is thus highly desirable to explore complementary platforms that offer greater control, cleaner environments, and more direct observables.

In this manuscript, we propose that strongly interacting two-component atoms offer a versatile and controllable platform to investigate dipole condensates coupled to rank-2 electric fields. The setup illustrated in Fig. 1 consists of atoms with two internal states or two species of atoms, which are labeled by pseudospin $\sigma = \uparrow, \downarrow$. With its high tunability and disorder-free environment, this setup enables unambiguous diagnosis of dipole condensation and allows for the controlled application of synthetic tensor gauge fields. To be more specific, in the presence of strong interactions, a single particle in neither spin could move. Instead, a particle from one component and a hole from the other form a dipole and a dipole con-

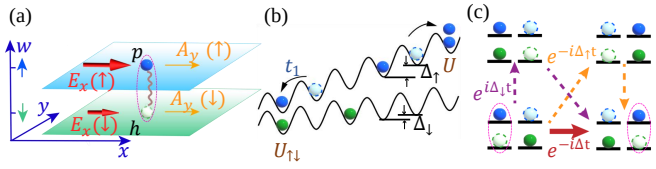

FIG. 1. (a) Spin-up (blue) and spin-down (green) atoms are regarded as two different layers in the synthetic dimension denoted by w. Spin-dependent effective electric field $E_x(\sigma)$ provides a dipole (ellipse) with a rank-2 electric field E_{xw}. (b) An optical lattice with a spin-dependent linearly tilt $\Delta_\uparrow \neq \Delta_\downarrow$. (c) The hopping of a dipole through second order processes $\sim e^{-i\Delta t}$ in the large U limit, where $\Delta = \Delta_\uparrow - \Delta_\downarrow = E_{xw}$.

* zhou753@purdue.edu
† shaoliang@hust.edu.cn

densate arises as the ground state. By interpreting the pseudospin as a synthetic dimension denoted by w, these two components are effectively separated from each other along w. A spin-dependent force in the x-direction corresponds to an effective electric field $E_x(\sigma)$, as shown in Fig. 1(a), and thus leads to a finite gradient of E_x in the w direction. This gives rise to a discrete rank-2 electric field $E_{xw} = \partial_w E_x \sim E_x(\uparrow) - E_x(\downarrow)$.

Using this platform, we identify the atomic analog of the perfect Coulomb drag. Since it is more difficult to measure resistance than other quantities in atomic systems due to the absence of disorder, we demonstrate that tracking the displacement of the center of mass of each spin component reveals Coulomb drag-like behavior. As the intercomponent interaction increases, the displacements of the centers of mass of spin-up and spin-down atoms become equal in magnitude and opposite in direction, mimicking perfect Coulomb drag. Furthermore, we identify the smoking gun of the response of a dipole condensate to a rank-2 electric field. E_{xw} imprints a phase twist on the dipole condensate, generating a supercurrent of dipoles. In particular, this supercurrent obeys the dipolar Josephson relation and is governed by the phase gradient of the dipole condensate, enabling a direct experimental measurement of phase coherence of dipole condensates [26, 40].

Since a uniform tensor electric field induces dynamics of dipoles only along one direction, it is sufficient to consider a 1D Hamiltonian,

$$\hat{H}_B = \hat{K}_B + \hat{U}_B + \hat{V}_B, \tag{1}$$

where

$$\hat{K}_B = -t_1 \sum_{m,\sigma} (\hat{b}^\dagger_{m,\sigma} \hat{b}_{m+1,\sigma} + h.c.), \tag{2}$$

$$\hat{U}_B = \frac{U}{2} \sum_{m,\sigma} \hat{n}_{m,\sigma}(\hat{n}_{m,\sigma} - 1) + U_{\uparrow\downarrow} \sum_m \hat{n}_{m,\uparrow}\hat{n}_{m,\downarrow}, \tag{3}$$

$$\hat{V}_B = \sum_{m,\sigma} m\Delta_\sigma \hat{b}^\dagger_{m,\sigma}\hat{b}_{m,\sigma}. \tag{4}$$

$\hat{b}^\dagger_{m,\sigma}(\hat{b}_{m,\sigma})$ is the bosonic creation (annihilation) operator at site m for $\sigma = \uparrow, \downarrow$. U and $U_{\uparrow\downarrow}$ correspond to the amplitude of intra-spin and inter-spin on-site interaction respectively, and $\hat{n}_{m,\sigma} = \hat{b}^\dagger_{m,\sigma}\hat{b}_{m,\sigma}$. $\hat{V}_B$ denotes a spin-dependent linearly tilted potential as shown in Fig. 1(b). It is worth pointing out that $\hat{U}_B$ also describes bosons in the real space with long-range interactions. For instance, molecules or atoms with dipolar interactions could be placed in two separate layers [41, 42]. U then denotes the intra-layer onsite interaction and $U_{\uparrow\downarrow}$ denotes the inter-layer interaction.

Applying a unitary transformation, $\hat{\mathcal{U}}^\dagger \hat{H}_B \hat{\mathcal{U}}$, where $\hat{\mathcal{U}} = e^{i\hat{V}_B t/\hbar}$, $\hat{V}_B$ is eliminated in the time-dependent Schrödinger equation and the kinetic energy term $\hat{K}_B$ becomes time-dependent as $\hat{\tilde{K}}_B = -t_1 \sum_{m,\sigma}(e^{-i\Delta_\sigma t/\hbar}\hat{b}^\dagger_{m,\sigma}\hat{b}_{m+1,\sigma} + h.c.)$. This spin-dependent vector potential $A_\sigma = \Delta_\sigma t$ thus gives rise to a spin-dependent electric field $E_\sigma = \partial_t A_\sigma = \Delta_\sigma$, and a finite $E_{xw} = E_\uparrow - E_\downarrow$. Whereas $\hat{K}_B + \hat{U}_B$ is the standard Hamiltonian of two-component atoms in optical lattices, a spin-dependent tilt has also been realized experimentally [43]. By adding a magnetic field with a homogeneous gradient along the x direction, the Zeeman energy splitting between spin-up and spin-down atoms increases linearly with increasing m. A finite Δ/h is thus realized and its value could be tuned up to 10kHz, much larger than t_1/h, which is typically of the order of a few tens Hz or less. Our model in Eq.(1) is thus directly accessible in current experiments.

We first consider the ground state of $\hat{H}_B$ when $\Delta_\sigma = 0$. Previous studies have shown that the ground state is a dipole condensate, which was referred to as a counterflow superfluid in the parameter regime where $t_1 \ll U, U_{\uparrow\downarrow}$ [7, 44, 45]. A recent experiment has realized such a counterflow superfluid in optical lattices [46]. Here, we numerically compute the correlation functions of the ground state using density matrix renormalization group (DMRG) method [47]. We choose $N = N_\uparrow + N_\downarrow = L$, where N_σ is the particle number of spin σ, N is total particle number, and L is number of lattice sites. We observe that the one-body correlation function decays exponentially, $C_{mm',\sigma} = \langle \hat{b}^\dagger_{m,\sigma}\hat{b}_{m',\sigma}\rangle \sim e^{-|m-m'|/\xi}$, where ξ is the coherent length. Meanwhile, the reduced two-body density matrix decays as a power law,

$$C^D_{mm'} = \langle \hat{b}^\dagger_{m,\uparrow}\hat{b}_{m,\downarrow}\hat{b}_{m',\uparrow}\hat{b}^\dagger_{m',\downarrow}\rangle = \langle \hat{D}^\dagger_m \hat{D}_{m'}\rangle \sim |m-m'|^\alpha, \tag{5}$$

where we define $\hat{D}^\dagger_m = \hat{b}^\dagger_{m,\uparrow}\hat{b}_{m,\downarrow}$ as the creation operator of a dipole at site m, and the exponent α depends on the interaction strength. For instance, when $U = 2U_{\uparrow\downarrow} \gg t_1$, α approaches $-1/2$. These results confirm that the ground state here is indeed a dipole quasi-condensate in 1D.

We then turn on a finite $\Delta_\uparrow$ while $\Delta_\downarrow$ remains zero. This mimics the Coulomb drag experiments in bilayer systems where a voltage is applied to only one layer. The subsequent dynamics is numerically simulated using the time-evolution block-decimation (TEBD) method [47]. Snapshots of the density profiles $n_{m,\sigma}(t)$ are shown in Fig. 2. It is clear that spin-up atoms quickly moves to the left and their density profile changes significantly compared to the equilibrium result. In contrast, the density profile of spin-down atoms experiences only small changes if $U_{\uparrow\downarrow}$ is small, as shown in Fig. 2(a). However, the results become drastically different once we increase $U_{\uparrow\downarrow}$. In spite of a vanishing $\Delta_\downarrow$, Fig. 2(b) shows that the density profile of the spin down atoms also changes significantly compared to the equilibrium result. The increase (decrease) in the density of spin-up atoms is always accompanied by a symmetric decrease (increase) of spin-down atoms with respect to the equilibrium results. This is a direct consequence of the mutual interactions between spin-up and spin-down atoms that push spin-down atoms toward the opposite directions of spin-up atoms. Despite that atoms here interact with

each other via onsite interaction, unlike excitonic systems where long-range Coulomb interactions exist, such correlated dynamics of spin-up and spin-down atoms is an atomic analog of the Coulomb drag.

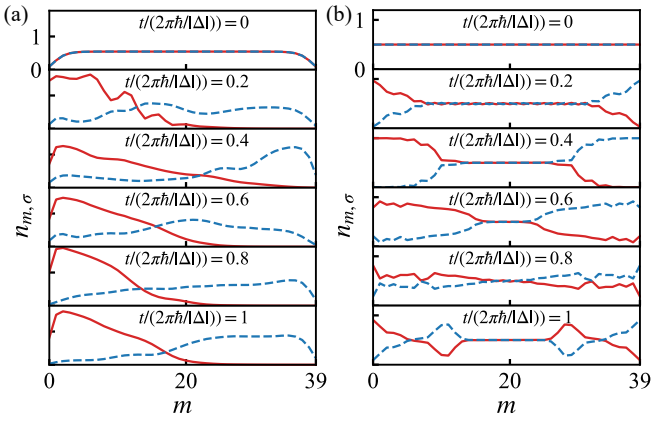

FIG. 2. Snapshots of the density profiles $n_{m,\sigma}(t)$ of spin-up (red solid line) and spin-down atoms (blue dashed line) in the presence of a spin-dependent electric field with $\Delta_\uparrow = 0.05t_1$ and $\Delta_\downarrow = 0$. The size of the chain is $L = 40$ with $N_\uparrow = N_\downarrow = L/2$. (a) and (b) illustrate weak and strong interactions, $U_{\uparrow\downarrow} = \frac{1}{2}U = 0.25t_1$ and $10t_1$, respectively.

To further quantitatively characterize the Coulomb-like drag in atomic systems, we evaluate the center of mass of each spin component,

$$X_\sigma = \sum_m m\langle \hat{n}_{m,\sigma}\rangle. \tag{6}$$

In Fig. 3, we show the displacement of X_σ from the initial value, $X_\sigma(t) - X_\sigma(0)$. In the presence of a finite $\Delta_\uparrow$, the center of mass of spin-up atoms $X_\uparrow$ exhibits a rapid change, which is accompanied by small oscillations due to a small but finite interaction with spin-down atoms $U_{\uparrow\downarrow}$, as shown in Fig. 3(a). Meanwhile, due to the absence of an electric field acting on spin-down atoms, i.e., $\Delta_\downarrow = 0$, the change of $X_\downarrow$ is much smaller, with a slight oscillation due to a finite but weak $U_{\uparrow\downarrow}$. In sharp contrast, in the large $U_{\uparrow\downarrow}$ limit, the dynamics of spin-down atoms are highly correlated to spin-up atoms. As shown in Fig. 3(b), when $U_{\uparrow\downarrow} = \frac{1}{2}U = 10t_1$, $X_\uparrow$ and $X_\downarrow$ oscillate with equal amplitudes and opposite signs.

To analyze the correlated dynamics of the spin-up and spin-down atoms, we consider the relative displacement between the spin-up particles and spin-down holes. We note that for the same spin component, the center of mass of holes differs from that of particles by a minus sign. Thus, we define

$$X_r = X_\uparrow - (-X_\downarrow) = X_\uparrow + X_\downarrow, \tag{7}$$

which characterizes the relative displacement of the particles in the top layer from the holes in the bottom layer in the x direction in Fig. 1(a). To quantitatively characterize how such displacement depends on $U_{\uparrow\downarrow}$ in the

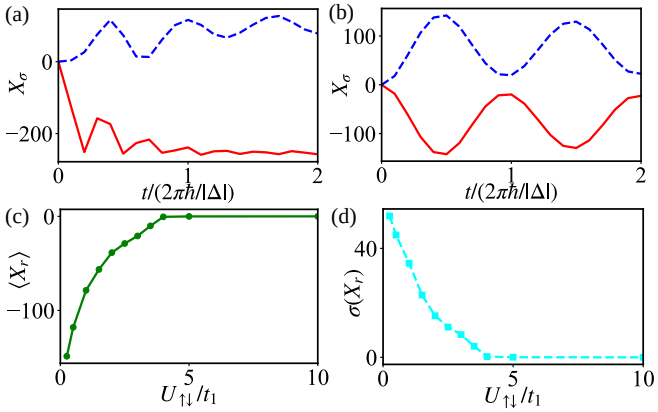

FIG. 3. (a,b) The displacement of the center of mass X_σ of spin-up (red solid line) and spin-down atoms (blue dashed line) in the presence of a spin-dependent electric field with $\Delta_\uparrow = 0.05t_1$ and $\Delta_\downarrow = 0$ when $U_{\uparrow\downarrow} = \frac{1}{2}U = 0.25t_1$ (a) and $U_{\uparrow\downarrow} = \frac{1}{2}U = 10t_1$ (b). The size of the chain is $L = 40$ with $N_\uparrow = N_\downarrow = L/2$. (c,d) Time-averaged relative displacement $\langle X_r\rangle$ and its variance $\sigma(X_r)$ as a function of the inter-spin interaction strength $U_{\uparrow\downarrow}$.

dynamics induced by $E_{xw} \sim \Delta_\uparrow - \Delta_\downarrow$, we define the time-averaged X_r and its variance:

$$\begin{aligned}\langle X_r\rangle &= \frac{1}{t}\int_0^t X_r(t')dt', \\ \sigma(X_r) &= \left\{\frac{1}{t}\int_0^t [X_r(t') - \langle X_r\rangle]^2 dt'\right\}^{1/2}.\end{aligned} \tag{8}$$

With increasing $U_{\uparrow\downarrow}$, $\langle X_r\rangle$ approaches 0, as shown in Fig. 3(c). Furthermore, $\sigma(X_r)$ also vanishes in the large $U_{\uparrow\downarrow}$ limit, as shown in Fig. 3(d). Since the integrand in the expression for $\sigma(X_r)$ is non-negative, a vanishing $\sigma(X_r)$ means that, once $\Delta_\uparrow$ drives oscillations of spin-up atoms, its center of mass is perfectly locked with the center of mass of holes in spin-down atoms at anytime, despite that spin-down atoms themselves are not subject to any finite $\Delta_\downarrow$. These results thus signify the atomic analog of perfect Coulomb drag in bilayer excitonic systems.

Whereas the above results allow us to explore Coulomb-like drag in atomic systems, phase coherence and superfluidity of the dipoles cannot be directly extracted from such information. We thus explore the supercurrent induced by a phase twist applied to the dipole condensate. To this end, we apply a strong rank-2 tensor electric field $\Delta = \Delta_\uparrow - \Delta_\downarrow$ for a short duration, in which the density of the atoms does not change. To understand how this field leads to a phase twist in the dipole condensate, we consider the effective model for dipoles in the strongly interacting regime.

As shown by Fig. 1(c), second-order processes exchange atoms with different spins on the nearest neighbor sites[7, 48]. An effective Hamiltonian is written as

$\hat{H}_E = \hat{K}_E + \hat{U}_E$ where

$$\begin{aligned}\hat{K}_E =& -\sum_m (t_2 e^{-i\Delta t/\hbar}\hat{b}^\dagger_{m,\uparrow}\hat{b}_{m,\downarrow}\hat{b}_{m+1,\uparrow}\hat{b}^\dagger_{m+1,\downarrow} + h.c.),\\ \hat{U}_E =& \tilde{U}\sum_m (\hat{n}_{m,\uparrow} - \hat{n}_{m,\downarrow})(\hat{n}_{m+1,\uparrow} - \hat{n}_{m+1,\downarrow}),\end{aligned} \tag{9}$$

$t_2 = 2t_1^2/U_{\uparrow\downarrow}$ is the amplitude of spin-exchange term, $\Delta = \Delta_\uparrow - \Delta_\downarrow$ is the rank-2 electric field, and $\tilde{U} = t_1^2(\frac{1}{U_{\uparrow\downarrow}} - \frac{2}{U})$ is the effective nearest-neighbor interaction strength [7]. In the language of synthetic dimension, t_2 becomes a ring-exchange interaction in the $x-w$ plane. The kinetic energy is rewritten as

$$\hat{K}_E = -\sum_m (t_2 e^{-i\Delta t/\hbar}\hat{D}^\dagger_m \hat{D}_{m+1} + h.c.). \tag{10}$$

In other words, a dipole sees a linearly growing vector potential or equivalently, a rank-2 electric field acting on a particle-hole pair.

Applying a strong rank-2 electric field to a dipole condensate for a short duration τ amounts to adding a phase to the ground state wavefunction $|G\rangle$,

$$|\Psi\rangle = e^{-i\sum_m m\Delta n_{m,D}\tau/\hbar}|G\rangle, \tag{11}$$

where $n_{m,D} = \langle G|\hat{D}^\dagger_m \hat{D}_m|G\rangle$ is the density of dipoles at site m. The phase $\Phi_{m,D} = m\Delta n_{m,D}\tau/\hbar$ is the consequence of the interplay between the dipole condensate and a linear potential $m\Delta$ generated by the rank-2 electric field, as shown in Fig. 4(a). The phase difference of the dipole condensate between the mth and $(m+1)$th sites, i.e., the phase gradient, is written as

$$\phi_{m,D} = [(m+1)n_{m+1,D} - mn_{m,D}]\tau\Delta/\hbar. \tag{12}$$

For a uniform density, $n_{m,D} = n_D$, the above expression can be simplified as

$$\phi_D = n_D\tau\Delta/\hbar. \tag{13}$$

At the end of this short pulse, though the densities of both spin components remain essentially unchanged, a finite ϕ_D induces supercurrents of dipoles on the link between the mth and $(m+1)$th sites,

$$J_D = 2t_2\rho_s^D \sin\phi_D, \tag{14}$$

where ρ_s^D is the superfluid density of dipoles. This equation is referred to as the dipolar Josephson relation [26, 40].

To test the above analytical results, we numerically compute the supercurent between the mth and $(m+1)$th sites using the full model $\hat{H}_B$ in Eq. (1),

$$J_D = 2t_2 \mathrm{Im}\langle \hat{D}^\dagger_m \hat{D}_{m+1}\rangle. \tag{15}$$

The post-pulse values of J_D are shown in Fig. 4(b). Because of the small variation of J_D across the whole system with nearly uniform density distribution, we have shown only the averaged J_D of the whole system in this figure. We see clearly that J_D is a sinusoidal function of ϕ_D and obeys the dipolar Josephson effect in Eq. (14). This is a hallmarking signature of a dipolar superfluid.

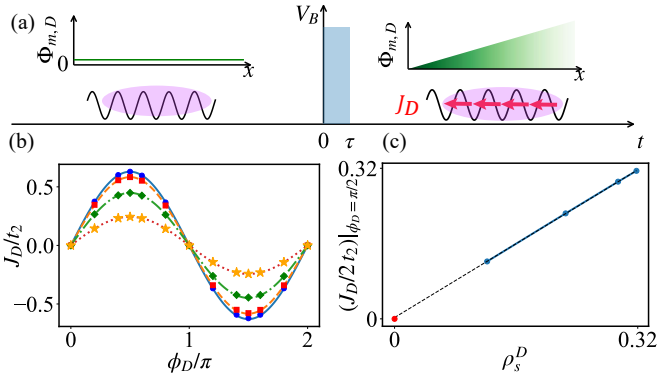

FIG. 4. (a) The scheme to generate dipolar supercurrents. A short pulse with amplitude $\Delta = \Delta_\uparrow - \Delta_\downarrow$, applied between $t = 0$ and $t = \tau$, generates a phase twist $\Phi_{m,D}$, which then induces supercurrents of dipoles J_D. (b) The dependence of J_D on the phase gradient ϕ_D at different dipole densities, $\rho = 0.125$ (orange stars), $\rho = 0.25$ (green diamonds), $\rho = 0.375$ (red squares) and $\rho = 0.5$ (blue circles). Curves are fittings to sinusoidal functions. (c) A comparison between numerical results of ρ_s^D and analytical results in Eq. (16).

It is also worth mentioning that ρ_s^D here has a simple analytical expression since dipoles can be treated as hard-core bosons in the large $U_{\uparrow\downarrow}$ limit. Furthermore, the nearest neighbor interaction in Eq. (9) can be made vanishingly small once $U_{\uparrow\downarrow} \to U/2$. For hardcore bosons, the superfluid density satisfies $\rho_s = \rho\sin(\pi\rho)/\pi$, where ρ_s is the superfluid density and ρ is the total density [49]. As such, ρ_s^D here satisfies

$$\rho_s^D = \rho_D \sin(\pi\rho_D)/\pi, \tag{16}$$

where ρ_D is the density of dipoles. To verify this relationship, we change $\rho_D = N_\uparrow/N$ by varying $N_\uparrow$ while keeping $N_\uparrow + N_\downarrow = L$ unchanged. We repeat the calculation of J_D for various ρ_D and extract ρ_s^D using $J_D/(2t_2)$ at $\phi_D = \pi/2$ in Eq. (14). We then compare these results with ρ_s^D obtained from the analytical relationship with ρ_D in Eq. (16). Fig. 4 (c) shows that these two results agree well with each other, further demonstrating the validity of the dipolar Josephson relation.

We emphasize that in the strongly interacting limit, J_D depends only on $\Delta = \Delta_\uparrow - \Delta_\downarrow$. We have verified that different choices of $\Delta_\uparrow$ and $\Delta_\downarrow$ at fixed Δ lead to the same J_D. When $\Delta_\uparrow = \Delta_\downarrow$, the rank-2 electric field vanishes and the system is subject to a uniform rank-1 electric field. We have found that J_D vanishes, confirming that a dipole condensate is decoupled from a vector gauge field.

In ultracold-atom experiments, J_D is directly observable. We define local spin operators $\hat{S}^z_m = (\hat{b}^\dagger_{m,\uparrow}\hat{b}_{m,\uparrow} - \hat{b}^\dagger_{m,\downarrow}\hat{b}_{m,\downarrow})/2$, $\hat{S}^x_m = (\hat{b}^\dagger_{m,\uparrow}\hat{b}_{m,\downarrow} + \hat{b}^\dagger_{m,\downarrow}\hat{b}_{m,\uparrow})/2$ and $\hat{S}^y_m = (\hat{b}^\dagger_{m,\uparrow}\hat{b}_{m,\downarrow} - \hat{b}^\dagger_{m,\downarrow}\hat{b}_{m,\uparrow})/(2i)$. Since $\hat{S}^\pm_m = \hat{S}^x_m \pm i\hat{S}^y_m$,

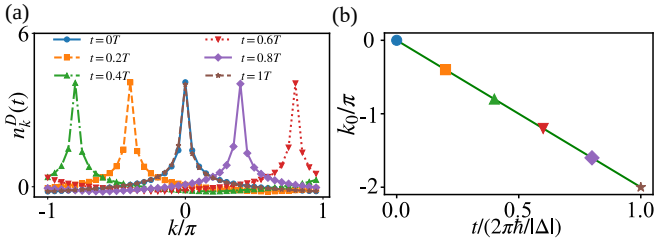

FIG. 5. (a) The momentum distribution of dipoles at different times. (b) The position of the maximum k_0 changes linearly with time. $L = 40$, $U_{\uparrow\downarrow} = \frac{1}{2}U = 20t_1$, and $\Delta = \Delta_\uparrow - \Delta_\downarrow = 0.6t_1$ have been used.

$\hat{S}_m^+ = \hat{b}_{m,\uparrow}^\dagger \hat{b}_{m,\downarrow}$, $\hat{S}_m^- = \hat{b}_{m,\downarrow}^\dagger \hat{b}_{m,\uparrow}$, the dipole correlation function $C_s = \langle \hat{D}_m^\dagger \hat{D}_{m+1}\rangle = \langle \hat{S}_m^+ \hat{S}_{m+1}^-\rangle$ is rewritten as

$$C_s = \langle \hat{S}_m^x \hat{S}_{m+1}^x\rangle + \langle \hat{S}_m^y \hat{S}_{m+1}^y\rangle + i(\langle \hat{S}_m^y \hat{S}_{m+1}^x\rangle - \langle \hat{S}_m^x \hat{S}_{m+1}^y\rangle). \tag{17}$$

The dipole current in Eq. (15) is then related to the spin-spin correlation functions, $J_D = 2t_2 \mathrm{Im} C_s$. A recent experiment has measured the first two terms in Eq. (17) [46]. Since $\langle \hat{S}_m^z \hat{S}_{m+1}^z\rangle$ corresponds to the density-density correlation $\langle \hat{n}_{m,\sigma}\hat{n}_{m+1,\sigma'}\rangle$, applying a global $\pi/2$ pulse, which rotates all spins about the x (y) axis before the density images are taken, $\langle \hat{S}_m^y \hat{S}_{m+1}^y\rangle$ ($\langle \hat{S}_m^x \hat{S}_{m+1}^x\rangle$) is thus obtained. The last two terms in Eq. (17) can also be measured using a straightforward generalization of this method. A site-selective $\pi/2$ pulse, which rotates spins on even sites about the x-axis (y-axis) and other spins on odd sites about the y-axis (x-axis) before taking the density images, directly provides $\langle \hat{S}_m^y \hat{S}_{m+1}^x\rangle$ ($\langle \hat{S}_m^x \hat{S}_{m+1}^y\rangle$).

In addition to the direct measurement of $\langle \hat{D}_m^\dagger \hat{D}_{m+1}\rangle$, the dipole current J_D can also be extracted from its continuity equation. If we use J_D to denote the supercurrent of dipoles on the link between the jth and the $(j+1)$th sites, $\langle \partial_t \hat{P}_L\rangle = -J_D$ is satisfied, where $\hat{P}_L = \frac{1}{2}\sum_{m<j+1}\langle \hat{n}_{m\uparrow} - \hat{n}_{m\downarrow}\rangle$ is the total dipole moment of all sites on the left hand side of the link of interest [26]. Measuring the time-dependent density distribution and the subsequent change rate in $\hat{P}_L$ then provide J_D.

An alternative means for studying the effect of rank-2 electric field is to consider the momentum distribution of dipoles. Similar to the momentum distribution of single-particles that is the Fourier transform of the single-body correlation function, we define the momentum distribution of dipoles,

$$n_k^D(t) = \frac{1}{L}\sum_{m,m'} \langle \hat{D}_m^\dagger \hat{D}_{m'}\rangle e^{ik(m-m')}. \tag{18}$$

As for the ground state, the momentum distribution is centered around $k = 0$. After applying the strong pulse of $\Delta \gg t_2$, the width of n_k^D remains unchanged, and the position of the center, characterized by k_0 in the Brillouin zone, shifts when t increases, as shown by Fig. 5(a). This is a signature of the Bloch oscillation of the dipole condensates induced by E_{xw}. The period of this dipolar Bloch oscillation is given by $T = 2\pi\hbar/|\Delta|$, as shown by Fig. 5.

In conclusion, we have shown that two-component atomic systems offer a highly tunable platform for studying the intriguing quantum phenomena induced by the coupling between dipole condensates and rank-2 electric fields. Pseudospin-dependent forces and strong interactions lead to the atomic analogy of perfect Coulomb drag and the dipolar Josephson effect, both of which are directly observable in current experiments. We hope that our results will stimulate more interest in studying the interplay of multipole condensates and higher-rank tensor gauge fields in synthetic quantum matter.

Acknowledgements: QZ acknowledges supports from National Science Foundation (NSF) through Grant No. PHY-2110614. SZ is supported by National Natural Science Foundation of China (Grant No.12174138). The DMRG and TEBD simulations were performed by using the Tensor Network Python (TeNPy) package developed by J. Hauschild and F. Pollmann [47] and were run on the HPC Platform of Huazhong University of Science and Technology.

[1] C. K. Law, H. Pu, and N. P. Bigelow, Quantum Spins Mixing in Spinor Bose-Einstein Condensates, Phys. Rev. Lett. **81**, 5257 (1998).
[2] T.-L. Ho and S. K. Yip, Fragmented and Single Condensate Ground States of Spin-1 Bose Gas, Phys. Rev. Lett. **84**, 4031 (2000).
[3] E. J. Mueller, T.-L. Ho, M. Ueda, and G. Baym, Fragmentation of Bose-Einstein condensates, Phys. Rev. A **74**, 033612 (2006).
[4] B. Evrard, A. Qu, J. Dalibard, and F. Gerbier, Observation of fragmentation of a spinor Bose-Einstein condensate, Science **373**, 1340 (2021).
[5] S. Musolino, H. Kurkjian, M. Van Regemortel, M. Wouters, S. J. J. M. F. Kokkelmans, and V. E. Colussi, Bose-Einstein Condensation of Efimovian Triples in the Unitary Bose Gas, Phys. Rev. Lett. **128**, 020401 (2022).
[6] H. Pu and N. P. Bigelow, Properties of Two-Species Bose Condensates, Phys. Rev. Lett. **80**, 1130 (1998).
[7] A. B. Kuklov and B. V. Svistunov, Counterflow Superfluidity of Two-Species Ultracold Atoms in a Commensurate Optical Lattice, Phys. Rev. Lett. **90**, 100401 (2003).
[8] Q. Zhou, J. V. Porto, and S. Das Sarma, Condensates induced by interband coupling in a double-well lattice, Phys. Rev. B **83**, 195106 (2011).
[9] Z. Zhang, L. Chen, K.-X. Yao, and C. Chin, Transition from an atomic to a molecular Bose–Einstein condensate, Nature **592**, 708 (2021).

[10] N. Bigagli, W. Yuan, S. Zhang, B. Bulatovic, T. Karman, I. Stevenson, and S. Will, Observation of Bose–Einstein condensation of dipolar molecules, Nature **631**, 289 (2024).

[11] I. B. Spielman, J. P. Eisenstein, L. N. Pfeiffer, and K. W. West, Resonantly Enhanced Tunneling in a Double Layer Quantum Hall Ferromagnet, Phys. Rev. Lett. **84**, 5808 (2000).

[12] J. Eisenstein and A. H. MacDonald, Bose–Einstein condensation of excitons in bilayer electron systems, Nature **432**, 691 (2004).

[13] J. Kasprzak, M. Richard, S. Kundermann, A. Baas, P. Jeambrun, J. M. J. Keeling, F. M. Marchetti, M. H. Szymańska, R. André, J. L. Staehli, V. Savona, P. B. Littlewood, B. Deveaud, and L. S. Dang, Bose–Einstein condensation of exciton polaritons, Nature **443**, 409 (2006).

[14] R. Balili, V. Hartwell, D. Snoke, L. Pfeiffer, and K. West, Bose-Einstein Condensation of Microcavity Polaritons in a Trap, Science **316**, 1007 (2007).

[15] J. P. Eisenstein, Exciton Condensation in Bilayer Quantum Hall Systems, Annual Review of Condensed Matter Physics **5**, 159 (2014).

[16] M. Kellogg, J. P. Eisenstein, L. N. Pfeiffer, and K. W. West, Vanishing Hall Resistance at High Magnetic Field in a Double-Layer Two-Dimensional Electron System, Phys. Rev. Lett. **93**, 036801 (2004).

[17] E. Tutuc, M. Shayegan, and D. A. Huse, Counterflow Measurements in Strongly Correlated GaAs Hole Bilayers: Evidence for Electron-Hole Pairing, Phys. Rev. Lett. **93**, 036802 (2004).

[18] D. Nandi, A. D. K. Finck, J. P. Eisenstein, L. N. Pfeiffer, and K. W. West, Exciton condensation and perfect Coulomb drag, Nature **488**, 481 (2012).

[19] Z. Wang, D. A. Rhodes, K. Watanabe, T. Taniguchi, J. C. Hone, J. Shan, and K. F. Mak, Evidence of high-temperature exciton condensation in two-dimensional atomic double layers, Nature **574**, 76 (2019).

[20] J. I. A. Li, T. Taniguchi, K. Watanabe, J. Hone, and C. R. Dean, Excitonic superfluid phase in double bilayer graphene, Nature Physics **13**, 751 (2017).

[21] C. Stahl, E. Lake, and R. Nandkishore, Spontaneous breaking of multipole symmetries, Phys. Rev. B **105**, 155107 (2022).

[22] E. Lake, M. Hermele, and T. Senthil, Dipolar Bose-Hubbard model, Phys. Rev. B **106**, 064511 (2022).

[23] E. Lake, H.-Y. Lee, J. H. Han, and T. Senthil, Dipole condensates in tilted Bose-Hubbard chains, Phys. Rev. B **107**, 195132 (2023).

[24] P. Zechmann, E. Altman, M. Knap, and J. Feldmeier, Fractonic Luttinger liquids and supersolids in a constrained Bose-Hubbard model, Phys. Rev. B **107**, 195131 (2023).

[25] S. A. Chen and P. Ye, Many-body physics of spontaneously broken higher-rank symmetry: from fractonic superfluids to dipolar Hubbard model (2023), arXiv:2305.00941 [cond-mat.str-el].

[26] W. Xu, C. Lv, and Q. Zhou, Multipolar condensates and multipolar Josephson effects, Nature Communications **15**, 4786 (2024).

[27] D. Jérome, T. M. Rice, and W. Kohn, Excitonic Insulator, Phys. Rev. **158**, 462 (1967).

[28] Y. Zeng, D. Sun, N. J. Zhang, R. Q. Nguyen, Q. Shi, A. Okounkova, K. Watanabe, T. Taniguchi, J. Hone, C. R. Dean, and J. I. A. Li, Evidence for a Superfluid-to-solid Transition of Bilayer Excitons (2023), arXiv:2306.16995 [cond-mat.mes-hall].

[29] M. Pretko, Subdimensional particle structure of higher rank $U(1)$ spin liquids, Phys. Rev. B **95**, 115139 (2017).

[30] H. Ma, M. Hermele, and X. Chen, Fracton topological order from the Higgs and partial-confinement mechanisms of rank-two gauge theory, Phys. Rev. B **98**, 035111 (2018).

[31] D. Bulmash and M. Barkeshli, Higgs mechanism in higher-rank symmetric U(1) gauge theories, Phys. Rev. B **97**, 235112 (2018).

[32] M. Pretko, Generalized electromagnetism of subdimensional particles: A spin liquid story, Phys. Rev. B **96**, 035119 (2017).

[33] M. Pretko, X. Chen, and Y. You, Fracton phases of matter, International Journal of Modern Physics A **35**, 2030003 (2020).

[34] S. Zhang, C. Lv, and Q. Zhou, Synthetic tensor gauge fields, Phys. Rev. Res. **7**, 013013 (2025).

[35] M. Kellogg, J. P. Eisenstein, L. N. Pfeiffer, and K. W. West, Bilayer Quantum Hall Systems at $\nu_T = 1$: Coulomb Drag and the Transition from Weak to Strong Interlayer Coupling, Phys. Rev. Lett. **90**, 246801 (2003).

[36] B. N. Narozhny and A. Levchenko, Coulomb drag, Rev. Mod. Phys. **88**, 025003 (2016).

[37] X. Liu, K. Watanabe, T. Taniguchi, B. I. Halperin, and P. Kim, Quantum Hall drag of exciton condensate in graphene, Nature Physics **13**, 746 (2017).

[38] R. Qi, A. Y. Joe, Z. Zhang, J. Xie, Q. Feng, Z. Lu, Z. Wang, T. Taniguchi, K. Watanabe, S. Tongay, and F. Wang, Perfect Coulomb drag and exciton transport in an excitonic insulator, Science **388**, 278 (2025).

[39] P. X. Nguyen, L. Ma, R. Chaturvedi, K. Watanabe, T. Taniguchi, J. Shan, and K. F. Mak, Perfect Coulomb drag in a dipolar excitonic insulator, Science **388**, 274 (2025).

[40] M. Rontani and L. J. Sham, Josephson oscillations between exciton condensates in electrostatic traps, Phys. Rev. B **80**, 075309 (2009).

[41] L. Du, P. Barral, M. Cantara, J. de Hond, Y.-K. Lu, and W. Ketterle, Atomic physics on a 50-nm scale: Realization of a bilayer system of dipolar atoms, Science **384**, 546 (2024).

[42] W. G. Tobias, K. Matsuda, J.-R. Li, C. Miller, A. Carroll, T. Bilitewski, A. M. Rey, and J. Ye, Reactions between layer-resolved molecules mediated by dipolar spin exchange, Science **375**, 1299 (2022).

[43] M. Aidelsburger, M. Atala, M. Lohse, J. T. Barreiro, B. Paredes, and I. Bloch, Realization of the Hofstadter Hamiltonian with Ultracold Atoms in Optical Lattices, Phys. Rev. Lett. **111**, 185301 (2013).

[44] A. Kuklov, N. Prokof'ev, and B. Svistunov, Superfluid-Superfluid Phase Transitions in a Two-Component Bose-Einstein Condensate, Phys. Rev. Lett. **92**, 030403 (2004).

[45] A. Hu, L. Mathey, I. Danshita, E. Tiesinga, C. J. Williams, and C. W. Clark, Counterflow and paired superfluidity in one-dimensional Bose mixtures in optical lattices, Phys. Rev. A **80**, 023619 (2009).

[46] Y.-G. Zheng, A. Luo, Y.-C. Shen, M.-G. He, Z.-H. Zhu, Y. Liu, W.-Y. Zhang, H. Sun, Y. Deng, Z.-S. Yuan, and J.-W. Pan, Counterflow superfluidity in a two-component Mott insulator, Nature Physics **21**, 208 (2025).

[47] J. Hauschild and F. Pollmann, Efficient numerical sim-

ulations with Tensor Networks: Tensor Network Python (TeNPy), SciPost Phys. Lect. Notes , 5 (2018).

[48] H.-N. Dai, B. Yang, A. Reingruber, H. Sun, X.-F. Xu, Y.-A. Chen, Z.-S. Yuan, and J.-W. Pan, Four-body ring-exchange interactions and anyonic statistics within a minimal toric-code Hamiltonian, Nature Physics **13**, 1195 (2017).

[49] M. Rigol, V. Rousseau, R. T. Scalettar, and R. R. P. Singh, Collective Oscillations of Strongly Correlated One-Dimensional Bosons on a Lattice, Phys. Rev. Lett. **95**, 110402 (2005).